https://doi.org/10.5194/essd-2023-259
Preprint. Discussion started: 11 October 2023
© Author(s) 2023. CC BY 4.0 License.

Open Access Earth System Science Data Discussions

Simbi: historical hydro-meteorological time series and signatures for 24 catchments in Haiti

Ralph Bathelemy[1,2*], Pierre Brigode[1,3], Vazken Andréassian[3], Charles Perrin[3], Vincent Moron[4], Cédric Gaucherel[5], Emmanuel Tric[1], Dominique Boisson[2]

[1] Université Côte d'Azur, Observatoire de la Côte d'Azur, CNRS, IRD, Géoazur, France
[2] Université d'Etat d'Haïti, Faculté des Sciences, LMI CARIBACT, Urgéo, Haïti
[3] Université Paris-Saclay, INRAE, HYCAR, Antony, France
[4] Aix Marseille University, CNRS, IRD, INRAE, CEREGE, Aix-en-Provence, France
[5] AMAP, INRAE, University of Montpellier, CNRS, IRD, Cirad, Montpellier, France

***correspondence:** Ralph Bathelemy (bathelemy@geoazur.unice.fr)

Abstract

The Caribbean country of Haiti is highly exposed to hydroclimatic hazards. However, there is no usable database that is easily accessible to the scientific community for this area. To fill this gap, hydroclimatic data were collected to create the first historical database in Haiti. This database, called "Simbi" (guardian of rivers, freshwater, and rain in Haitian mythology), includes 156 monthly rainfall series over the period 1905–2005, 59 daily rainfall series over the period 1920–1940, 70 daily streamflow series, and 23 monthly temperature series, not necessarily continuous, over the period 1920–1940. It also provides simulated streamflow series over the period 1920–1940 using the GR2M and GR4J rainfall–runoff models for 24 catchments and 48 attributes covering a wide range of topographic, climatic, geological, land use, hydrogeological, and hydrological signature indices. The database will be regularly updated to include additional historical data that will be digitized in the future. It will thus contribute toward better knowledge of the hydrology of Haitian catchments and will enable the implementation of various hydrological calculations useful for designing structures or flow forecasting. Simbi is an open access database and is available for download at: https://doi.org/10.23708/02POK6 (Bathelemy et al., 2023).

1 Introduction

Hydroclimatic databases, generally composed of climatic (precipitation and air temperature) and hydrological (streamflow) time series at the catchment scale, are extremely useful (Tramblay et al., 2021). They are used for water resources planning and management as well as for monitoring and forecasting floods, droughts, and changes in surface and groundwater resources (Dewandel et al., 2003, 2004; Alfieri et al., 2020; Harrigan et al., 2020).These databases are also used to evaluate the performance of "new" hydro-meteorological products based on Earth observation satellites, which are increasingly applied in poorly instrumented regions (Beck et al., 2019; Brocca et al., 2019; Prakash, 2019; Bathelemy et al., 2022). Furthermore, they are central to studies of climate change impact, for example, through the calibration and evaluation of hydrological models used to quantify climate change impacts on water resources (Abbaspour et al., 2009; Chokkavarapu and Mandla, 2019; Teutschbein and Seibert, 2012).

In recent years, hydroclimatic databases called "CAMELS" (catchment attributes and meteorology for large-sample studies) have been created in several countries: United States (Addor et al., 2017), Chile (Alvarez-Garreton et al., 2018), Brazil (Chagas et al., 2020), Great Britain (Coxon et al., 2020), Australia (Fowler *et al.*, 2021), Central Europe (Klingler et al., 2021), and Switzerland (Höge et al., 2023). The CAMELS databases use large datasets (precipitation, streamflow, air temperature, etc.) from multiple sources (in situ, reanalysis, remote sensing, etc.) over several hundreds of catchments. They also include multiple catchment attributes covering a range of topographic, climatic, hydrological, geological, and land use variables, etc. While the CAMELS databases provide time series, other databases provide indices and hydroclimatic signatures of

https://doi.org/10.5194/essd-2023-259
Preprint. Discussion started: 11 October 2023
© Author(s) 2023. CC BY 4.0 License.

catchments, such as the African Database of Hydrometric Indices (ADHI; Tramblay *et al.*, 2021). The main objective of these works is to make hydroclimatic data freely and easily available to the scientific community.

Unfortunately, there are significant differences between countries in terms of the quality and quantity of hydroclimatic reference databases, as well as regarding access to these data. Some countries do not have such reference databases. This is the case of Haiti, whose territory is, nevertheless, highly exposed to natural disasters (Khouakhi et al., 2017; Burgess et al., 2018), and which will, moreover, tend to increase due to climate change (Peterson et al., 2002). At the same time, Haiti is facing the consequences of massive deforestation and anarchic urbanization in recent decades (Hedges et al., 2018; Tarter et al., 2018; Mompremier et al., 2022), resulting in increased vulnerability to hydroclimatic hazards. Currently, there is no freely and easily accessible hydroclimatic database in Haiti. The only existing data are the 156 monthly rainfall series (1905–2005) compiled by Moron *et al.*, (2015), the 70 daily streamflow series (1920–1940) from the BVH project (*Bassins versants haïtien* in French, i.e., Haitian catchments; Gaucherel *et al.* 2018), paper archives in several institutions, and data collected as part of different projects, often available for very short periods. This BVH project includes the characterization of Haitian catchments using streamflow data (Gaucherel *et al.*, 2016) and rainfall data (Moron et al., 2015). The BVH has also investigated existing relationships between catchment shape, relief, and river sinuosity (Gaucherel *et al.*, 2017, Bonhomme *et al.*, 2013). These two databases (rainfall and streamflow data) are not known to the public, have never been cross-referenced to form a hydroclimatic database for the analysis of Haitian catchments, and remain largely underused to date.

The main goal of this study is to cross-reference and analyze these different databases in order to propose the first hydroclimatic database for several Haitian catchments. Nevertheless, most of the available historical Haitian streamflow series have gaps and are therefore limited in their application. One way to obtain continuous streamflow series is to use a hydrological model, fed by climatic time series, to reconstruct the missing values (Brigode et al., 2016; Smith et al., 2019). This method has been used for several decades for various types of catchments covering different climatic regions (Caillouet et al., 2017; Crooks and Kay, 2015; Jones and Lister, 1998). Thus, monthly (GR2M, Mouelhi *et al.*, 2006) and daily (GR4J, Perrin *et al.*, 2003) lumped rainfall–runoff models were used to reconstruct continuous streamflow series in Haiti at both time steps.

The goal of our work is therefore threefold:

i) producing climatic (air temperature and rainfall) series at the catchment scale by spatially and temporally aggregating available series,

ii) creating a continuous Haitian hydroclimatic database for the 1920–1940 period, using the catchment climatic series and the rainfall–runoff models,

iii) characterizing the hydrological behavior of Haitian catchments based on 48 hydrological indices and signatures covering six classes of catchment attributes (topographic, geological, hydrogeological, land use, climate indices, and hydrological signatures).

Observed hydroclimatic data, simulated streamflow series, and calculated catchment attributes make up the Simbi database, the first continuous and freely available hydrological database in Haiti. Simbi is a guardian of rivers, freshwater, and rain in Haitian mythology (https://en.wikipedia.org/wiki/Simbi).

2 Data used

2.1 Streamflow

The streamflow data consist of 70 daily series, most of which are available from 1920 to 1940, with significant gaps in some series. These data were collected by the *Hydrographic Department of the Irrigation Service of*

https://doi.org/10.5194/essd-2023-259
Preprint. Discussion started: 11 October 2023
© Author(s) 2023. CC BY 4.0 License.

the General Direction of Public Works in Haiti. On average, 12 gauging measurements were acquired per station and per year. These data were initially available in paper form in annual hydrographic bulletins. In the 1980s, a private company (LGL génie conseil) digitized these bulletins for the Haitian government. These data have not yet been used by the scientific community.

2.2 Rainfall

2.2.1 Monthly rainfall

A modified version of the monthly rainfall database compiled by Moron *et al.* (2015) was used in this study. The modifications to the original database are described in detail in Appendix A. The original data produced by Moron *et al.* (2015) included 156 monthly rainfall series available from 1905 to 2005 and were derived from three different sources:

1. The CNIGS (*National Center for Geospatial Information*) database with 162 monthly rainfall series;
2. The database managed by the international company *Chemonics* (https://chemonics.com/, accessed 06/02/2023) with 109 monthly rainfall series;
3. The CNSA (*National Coordination for Food Security*) database with 14 monthly rainfall series.

These three databases were merged by Moron *et al.* (2015) by removing and/or correcting duplicates. In total, 156 monthly rainfall series were validated and retained to form the monthly rainfall database. However, several series have a high percentage of missing data, and most of them have data available only from 1930 to 1970.

2.2.2 Daily rainfall

Several daily rainfall series were collected by the observatory of the Petit-Séminaire Collège St-Martial (PSCSM) in Port-au-Prince during the 20th century. These data were available in paper archives of the Haitian Spiritual Library (BHS for *Bibliothèque Haïtienne des Spiritains*) in Port-au-Prince. Overall, 59 of these series with data for the period 1920–1940 have been digitized for the Simbi database.

2.2.3 NOAA 20CR reanalysis rainfall

The third version of the *National Oceanic and Atmospheric Administration* (NOAA) Twentieth Century Reanalysis (20CR) project precipitation data (Slivinski et al., 2019) was used for the period 1920–1940. These data are available at a daily time step at a spatial scale of 1° (111 km at the equator). These are not measured data, but rainfall data from a global climatic model (reanalysis).

2.3 Air temperature

2.3.1 Digitization of historical archives

Air temperature data are available at a monthly time step in paper archives in the same river bulletins that contain streamflow data. A total of 23 monthly temperature series with data available for the period 1926–1939 have been digitized for the Simbi database. These temperature series are not continuous over time and there are significant gaps in some series.

2.3.2 NOAA 20CR reanalysis air temperature

The NOAA reanalysis air temperature database (Slivinski et al., 2019) was used in this study. This air temperature database is available at the same spatiotemporal resolution as the NOAA rainfall data (see section 2.2.3).

https://doi.org/10.5194/essd-2023-259
Preprint. Discussion started: 11 October 2023
© Author(s) 2023. CC BY 4.0 License.

2.3.3 Berkeley Earth Surface Temperature (BEST)

The BEST product was used, as retrieved from the http://berkeleyearth.org/ website (Muller et al., 2014). BEST is a gridded air temperature reanalysis for lands, starting in 1753 at the monthly resolution, and in 1880 at the daily resolution, with a 1° spatial resolution.

2.4 Digital Elevation Model (DEM)

The digital elevation model used in this study is the Shuttle Radar Topography Mission (SRTM) of the *United States Geological Survey* (USGS) and the *National Aeronautics and Space Administration* (NASA). The digital elevation model was extracted for Haiti and is available at a spatial resolution of 90 m (Reuter et al., 2007).

3 Methodology

This section presents the methodology followed (i) to select the climate series used for producing catchment climatic series, (ii) to simulate continuous monthly streamflow series with GR2M for 24 catchments selected and daily streamflow series with GR4J for 21 of the 24 catchments where daily rainfall data were available, and (iii) to compute hydrological indices and signatures for the selected catchments.

The conceptual lumped GR2M and GR4J models are described in Appendix B. The KGE objective function (Kling–Gupta efficiency; Gupta *et al.* 2009) was used to evaluate the performance of both models. The KGE score is defined by the following analytical formula:

$$KGE = 1 - \sqrt{(1+r)^2 + (1-\alpha)^2 + (1-\beta)^2} \quad (1)$$

where r is the correlation coefficient, α is the ratio of the standard deviation of the simulated streamflow to the standard deviation of the observed streamflow, and β is the ratio of the mean of the simulated streamflow to the mean of the observed streamflow.

3.1 Selection of streamflow data and catchments

3.1.1 Selection of streamflow series

An analysis of the 70 available streamflow series was performed to select the "hydrologically relevant" streamflow series. It resulted in the selection of 24 series. Four criteria were used to make this selection:

1. The annual hydrographic bulletins reported the accuracy with which rating curves were established through three ratings: "well established," "fairly well established," and "poorly established." Most of the streamflow series with "poorly established" rating curves were found to have significant measurement differences between periods. Therefore, the nine streamflow series with "poorly established" rating curves were not used in the remainder of this study.
2. Three hydrometric stations were located downstream of diversion channels or small dams used for irrigation. These streamflow series poorly represent the seasonality of streamflow, and are therefore considered to be influenced by human activities. These streamflow series were not used in the remainder of this study.
3. Eleven hydrometric stations were located downstream of resurgences or springs. These groundwater resurgences are beyond the scope of this work, which is limited to surface streamflow. Therefore, these streamflow series were not used in the remainder of this study.
4. The 23 streamflow series that had less than 5 years of data were not used in the remainder of this study.

https://doi.org/10.5194/essd-2023-259
Preprint. Discussion started: 11 October 2023
© Author(s) 2023. CC BY 4.0 License.

3.1.2 Catchment boundaries and areas

The contours of the 24 catchments corresponding to the 24 selected hydrometric stations were delineated using the SRTM digital terrain model (Reuter et al., 2007) and the TauDEM algorithm (Tarboton et al., 2005). Numerically calculated catchment areas were compared with those reported in river bulletins (areas estimated from U.S. Army maps). Two factors account for significant differences between the two areas:

1. The exact positions of the hydrometric stations are not known. Some stations have been relocated manually based on information in the hydrographic bulletins (name of a bridge, main road, monuments, etc.),
2. Due to the low resolution of the numerical model used, the numerically obtained streamflow may differ from the actual streamflow, especially in plain areas near the estuaries. Hydrometric stations were therefore placed on the digitized rivers.

The station relocation process was repeated several times until the error between the two areas was less than 10%. The geographic locations of the 24 selected hydrometric stations are shown as red dots in Figure *1*.

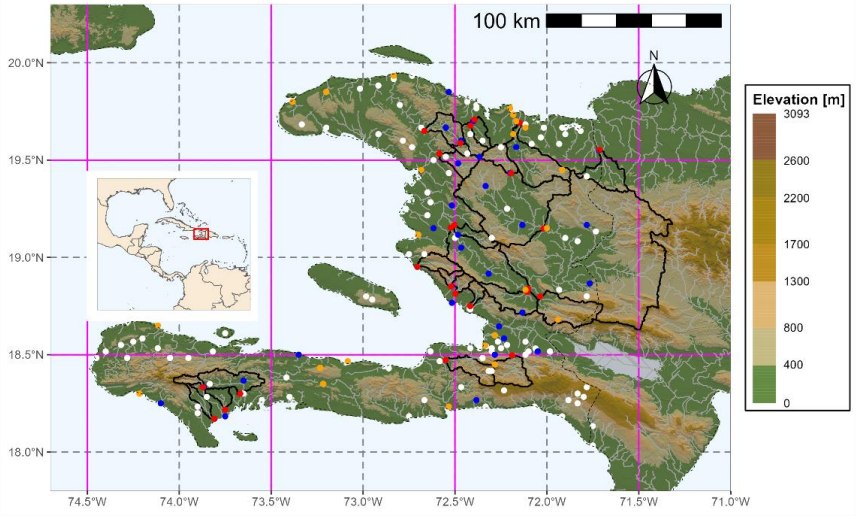

Figure 1 – Location of the 24 hydrometric stations used (red dots), the associated catchment contours (black solid lines), and the location of all rain gauges with monthly data for the period 1920–1940 (white, orange, and blue dots). Raingauge stations with air temperature data are shown in orange. Raingauges considered relevant for hydrological modeling are shown in blue (see section 3.2.1). NOAA 20CR pixels are shown in purple, the border between Haiti and the Dominican Republic is shown as a dashed black line, and the background topography is from the SRTM database.

3.2 Building catchment climate series

3.2.1 Rainfall

For each catchment, the most relevant raingauges for rainfall–runoff modeling were identified. The performance of a rainfall–runoff model is known to improve with a better description of the rainfall inputs to the catchment (Andréassian et al., 2001). Therefore, GR2M was used as an analytical tool to select the most relevant raingauge combination for each catchment.

Three types of rainfall data were used as inputs to GR2M: (i) NOAA 20CR rainfall data, (ii) data from all available raingauges, and (iii) data from several possible combinations of raingauges.

https://doi.org/10.5194/essd-2023-259
Preprint. Discussion started: 11 October 2023
© Author(s) 2023. CC BY 4.0 License.

1. NOAA 20CR rainfall data

Catchment-scale rainfall series were calculated as a weighted average of NOAA 20CR rainfall. The weights are proportional to the area of the NOAA pixel overlapping the catchment. The areas of most catchments are significantly smaller than the NOAA 20CR pixel. Thus, neighboring catchments located on the same NOAA grid cell will have the same rainfall series (see Figure *1*).

2. Reference rainfall at the catchment scale

For each catchment, an initial rainfall series, called "reference rainfall," was calculated as a weighted average of monthly rainfall data from Thiessen polygons (Croley and Hartmann, 1985; Han and Bray, 2006). Due to the high percentage of missing data in most rainfall series, the weights obtained from the Thiessen polygons were adjusted according to the data available at each time step: raingauges with missing data for a month m are not used for that month, and only raingauges with data for that month m are considered. This procedure has the disadvantage of potentially introducing non-stationarity in the catchment rainfall series according to the percentage of missing data for each raingauge. The low density of raingauges and the high spatial variability of rainfall in Haiti (Moron et al., 2015) make it difficult to apply methods to estimate missing data (Benoit et al., 2022; Di Piazza et al., 2011; Oriani et al., 2020). Therefore, gap-filling methods were not used.

3. Multiple raingauge combinations

All possible raingauge combinations are calculated for each catchment (combination of 1, 2, 3,..., n raingauges, where n is the number of available raingauges). The catchment scale rainfall is calculated for each of the raingauge combinations using Thiessen polygons. Since the raingauges used do not always have continuous records, some combinations of raingauges lead to gaps in catchment-scale rainfall series, which is a problem for continuous rainfall–runoff modeling. In the following, only continuous (gapless) catchment rainfall series were used for rainfall–runoff modeling.

4. Rainfall–runoff modeling for selecting the most relevant raingauge combination

The first 3 years of data (early 1920 to late 1922) were used to initialize the model internal states, and the remaining data were divided into two subperiods with the same available streamflow lengths to perform a calibration–evaluation procedure of parameter sets, as proposed by Klemeš (1986). The "Period 1" (resp. "Period 2") test corresponds to the use of the first (resp. second) half of available data for calibration and the second (resp. first) half for evaluation. The combination of raingauges with the best KGE score in the evaluation was considered the most relevant for rainfall–runoff modeling.

The KGE values obtained with the different combinations of raingauges are dependent on the model used and therefore do not represent the truth of what the "rainfall relevant for rainfall–streamflow modeling" catchment should be. A different model may produce different results.

3.2.2 Air temperature and potential evapotranspiration

The only observed air temperature series are available at a monthly time step and are not available for the entire study period (1920–1940). In our context, continuous air temperature series are needed to estimate potential evapotranspiration (PET) series at the catchment scale. Because the temperature series are incomplete, an annual-mean temperature was calculated for each station and used in the rainfall–runoff model.

Several studies have evaluated the impact of imperfect knowledge of temperature data (using annual averages in our study) on the performance of rainfall–runoff models (Burnash, 1995; Fowler, 2002; Kribèche, 1994). The results converge to show that this source of uncertainty is the least important and that it can be largely compensated by the model during calibration. To verify this hypothesis, two complementary temperature databases (NOAA 20CR and BEST) were used as inputs to the GR2M model. The aim is to test whether the performance of the model (KGE score) is sensitive to strong differences in temperature data.

1. Using NOAA 20CR and BEST air temperature

https://doi.org/10.5194/essd-2023-259
Preprint. Discussion started: 11 October 2023
© Author(s) 2023. CC BY 4.0 License.

Catchment temperature series were calculated at the daily time step as a weighted average of the NOAA 20CR and BEST air temperatures. The weights are proportional to the area of the NOAA 20CR or BEST pixel overlapping the catchment.

2. Using available meteorological stations

Annual-mean temperature series were calculated for each catchment at the monthly time step using the observed (digitalized data) temperatures. Daily temperature series were then derived by interpolation from a second-degree polynomial. A similar work of interpolation of monthly temperature series to obtain daily temperatures was performed by Andréassian *et al.* (2004). Daily temperature series at the catchment scale were calculated using the interpolated daily temperature series and Thiessen polygons (Croley and Hartmann, 1985; Han and Bray, 2006).

3. PET catchment series

The PET series are calculated using the formula of Oudin *et al.* (2005), which is based on air temperature. This formula was chosen for the calculation of PET for two main reasons. The other climate variables commonly used to calculate PET (wind speed, humidity, radiation, etc.) are unavailable, which justifies the use of a formula based only on temperature in a context where data are scarce. Moreover, it is one of the most relevant methods for rainfall–runoff modeling compared to 27 models for calculating PET and has been tested on more than 300 catchments covering several climatic zones, including tropical zones (Oudin et al., 2005), as is the case in Haiti. It uses as inputs the series of air temperature at the catchment scale and the average latitude of the catchments to calculate extraterrestrial radiation.

3.3 Water balance

The water balance was used as a complementary analytical tool to the GR2M model. The annual average water balance was presented in the form of a Turc–Budyko diagram, as described by Coron *et al.* (2015), for all 24 study catchments.

3.4 Simulation of monthly and daily streamflow series for the period 1920–1940

For each catchment, three sets of parameters were used to simulate the streamflow series over the period 1920–1940. The first two sets of parameters called “Period 1” and “Period 2,” respectively, are those described in section 3.2.1 and are obtained by calibration over the two subperiods from the catchment rainfall calculated from the raingauges considered most relevant and the PET series calculated from the digitized temperature series. The third set of parameters called “Period 3” is obtained by calibration over the whole period 1920–1940 (the first 3 years being used for model warm-up). The GR2M model was used to simulate the monthly streamflow series for the 24 basins studied, and the GR4J model was used to simulate the daily streamflow series for 21 of the 24 catchments where daily rainfall data are available. Modeling was performed using the airGR package (Coron et al., 2017, 2023) and R software (R Core Team, 2022).

3.5 Calculation of catchment attributes

Similar to the CAMELS databases (Addor *et al.*, 2017, Alvarez-Garreton *et al.*, 2018, Chagas *et al.*, 2020, Coxon *et al.*, 2020, Fowler *et al.*, 2021, Klingler *et al.*, 2021), several attributes were calculated for each catchment. Thus, 48 attributes grouped into six classes (topography, geology, land use, land acquisition type, climate index, and hydrological signature) were calculated (see Table *C2* in Appendix C). These attributes were selected according to the data available in Haiti and their relevance to Haitian catchments.

The catchment contours defined in section 3.1.2 and the SRTM digital terrain model with a resolution of 90 m (Reuter et al., 2007) were used to calculate the topographic attributes. The location of the catchment outlets was defined by the relocation process described in section 3.1.2. The hydrological signatures were calculated on the observed streamflow series and on the three simulated streamflow series with the three sets of

https://doi.org/10.5194/essd-2023-259
Preprint. Discussion started: 11 October 2023
© Author(s) 2023. CC BY 4.0 License.

calibration parameters (see section 3.4). Thus, there are four indicators for each of the hydrological signatures (one indicator for observed streamflow and three indicators for simulated streamflow).

The data used to produce the geological attributes, land cover characteristics, and aquifer types are produced by the CNIGS (*Centre National de l'Information Géospatiale*) and the BME (*Bureau des Mines et de l'Energie*). These data are freely available via the link (https://haitidata.org/, accessed on 08/12/2022). Unfortunately, no documentation exists for these data, with the exception of the geological data, which are very well documented (Boisson & Pubellier, 1987, Butterlin, 1960, Terrier *et al.*, 2014). Land use data are available for 1995 and 1998. We did not have land use data for the most recent period (2010–2022), let alone for the study period (1920–1940). Land use has changed significantly in recent decades, mainly due to massive deforestation and uncontrolled urbanization (Churches et al., 2014; Hedges et al., 2018; Salomon et al., 2022). Although the past (1920–1940) and the current land (2000–2020) cover is not what it was in 1995 and 1998, we have nevertheless chosen to present two land cover attributes calculated over these periods. For each catchment, the geological, land use, and aquifer type layers of the shapefile are cut out to enable the determination of the various corresponding attributes. Table C3 in Appendix C shows the lithology types, aquifer types, and land cover types.

4 Results

4.1 Impact of air temperature and PET series on rainfall–runoff modeling

Figure 2 shows (i) the relationship between digitized air temperatures (BHS) and the 20CR and BEST reanalyses (top three plots) as well as (ii) the performance (KGE score) and parameters of the GR2M model (bottom three plots) using the three air temperature databases to compute PET series. BEST overestimates the mean temperature (symbolized by the red dots in the boxplots in Figure 2, top left) and 20CR has difficulty representing temperatures below 20°C and over 28°C. The low dispersion (upper middle figure) of 20CR and BEST may be due to a spatial averaging effect at the scale of the grid boxes (1° for both), which are large for the study area. In addition, there is no linear correlation between the two temperature databases, and the 20CR data are a poor representation of the seasonal temperature variability in Haiti (upper right figure).

Although there is no clear correlation between the digitized and reanalyses temperatures, the KGE values (KGE in the evaluation for the two subperiods) obtained with the three air temperature databases are very similar for most of the catchments (bottom left figure). This shows that the GR2M model, through its two parameters and especially the X2 parameter (bottom right figure), has the ability to absorb the potential biases associated with the air temperature data.

The three temperature databases could be used a priori for rainfall–runoff modeling, as the model parameters absorb the associated biases. However, since the reanalysis databases do not represent temperature well at the catchment scale, they will not be used in the remainder of this study. Therefore, the digitized temperatures will be used to build the Simbi database.

https://doi.org/10.5194/essd-2023-259
Preprint. Discussion started: 11 October 2023
© Author(s) 2023. CC BY 4.0 License.

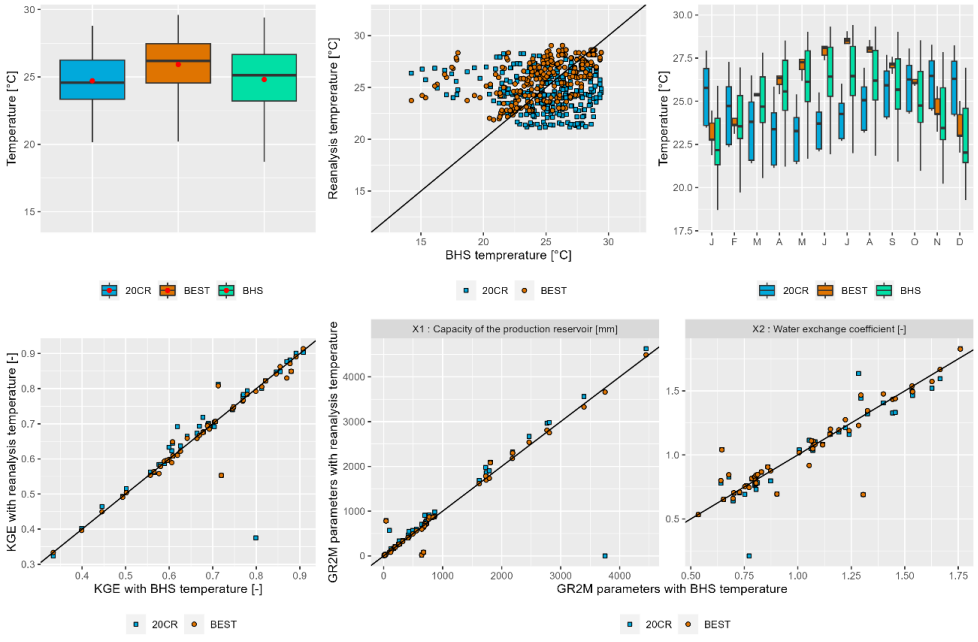

Figure 2 – Top left to right: Synthesis of monthly temperatures from the digitized archive (BHS) and reanalyses as a boxplot, plot of monthly temperatures from reanalyses versus digitized, seasonal temperature variability as a boxplot (each boxplot represents monthly temperatures for all basins). Bottom left to right: KGE values in the evaluation for the two subperiods and GR2M parameters X1 and X2 calculated with the two temperature databases.

4.2 Selection of relevant raingauges

4.2.1 GR2M performance analysis

Reference rainfall and rainfall from all possible combinations of raingauges were calculated at the catchment scale as described in section 3.2.1. Table C1 in Appendix C presents the number of raingauges used to calculate reference rainfall, the number of combinations, and the most relevant raingauges for rainfall–runoff modeling for each of the catchments.

Figure 3 shows the summary of the KGE scores in the evaluation and its three components obtained with NOAA 20CR rainfall, reference rainfall, and relevant raingauge combination. The lowest KGE scores are obtained with NOAA 20CR rainfall, highlighting the limitations of this rainfall database for rainfall–runoff modeling in Haiti and the need to use observed data rather than reanalyses. There is also a clear improvement in KGE values when using the relevant raingauges compared to the reference raingauges. Nevertheless, some catchments have poor KGE scores in the evaluation, despite the use of relevant raingauges. Among the three components of the KGE, the correlation coefficient (r) contributes most to the improvement in model performance through the use of ground-based rainfall data. Indeed, there is a weak correlation between the simulated and observed streamflow obtained with NOAA 20CR rainfall data, and this correlation is greatly improved by using observed rainfall data (reference raingauges and relevant raingauges). On the other hand, the coefficients α and β, which represent variability and bias, respectively, contribute most to the improvement of the model performance using the relevant raingauges compared to the reference raingauges. The values of these coefficients are much more centered around the optimal value of 1 for the relevant raingauges, while they are more scattered for the reference raingauges.

https://doi.org/10.5194/essd-2023-259
Preprint. Discussion started: 11 October 2023
© Author(s) 2023. CC BY 4.0 License.

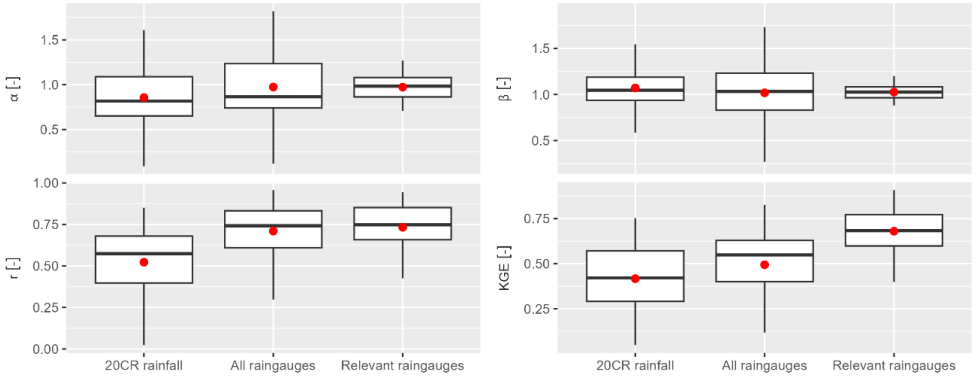

Figure 3 – Summary of KGE scores in the evaluation and its three components obtained with NOAA 20CR rainfall, reference rainfall, and relevant raingauges combination.

Figure *4* shows the spatial distribution of KGE scores in the evaluation using the three rainfall databases. As discussed earlier, the KGE scores in the evaluation with 20CR data are low, with only five catchments having KGE scores over 0.60. The performance (KGE score) improved for 21 catchments with the relevant raingauge combination, and no improvement was achieved for three catchments only: the catchments of Tumbe at Passe Fine (Q-044), Rivière du Sud at Camp-Périn (Q-008), and Coujol at Proby (Q-006). Two of these three catchments (Q-044 and Q-008) were already performing relatively well, with average KGEs in the evaluation over 0.60, and the use of the relevant raingauge combinations did not improve their performance further. Despite the use of relevant raingauges, four catchments have KGE values below 0.50, two of which have negative or near-zero KGE values: the Trois Rivières at Plaisance catchment (Q-051) and the Montrouis at Pont Toussaint catchment (Q-058).

https://doi.org/10.5194/essd-2023-259
Preprint. Discussion started: 11 October 2023
© Author(s) 2023. CC BY 4.0 License.

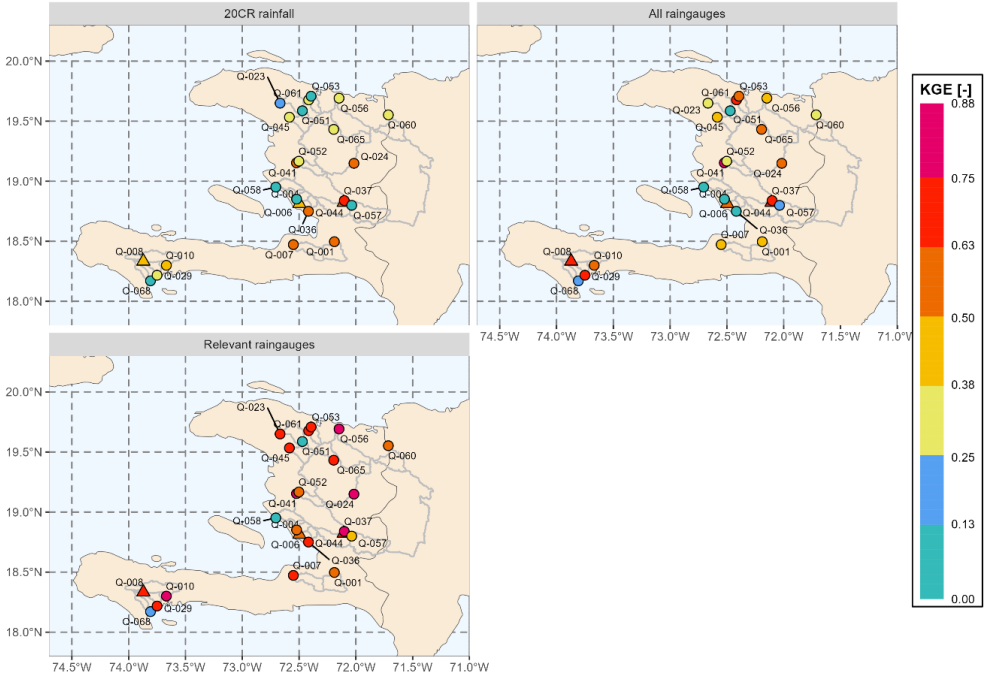

Figure 4 - Spatial distribution of the average of the two KGE values in the evaluation for the two subperiods. Dots represent catchments where model performance was improved by using the relevant raingauge combinations, triangles represent catchments where model performance was not improved by using the relevant raingauge combinations.

4.2.2 *Analysis of GR2M parameters*

In *Figure 5*, the influence of the relevant raingauge combinations on the stability of the model parameters is evaluated. The ratios of the calibration parameters of the two subperiods were plotted as a boxplot for the reference and relevant raingauge combinations. The results showed that the relevant raingauge combinations led to more stable X1 and X2 parameters (ratio close to 1). In fact, the length of the boxplot of the reference raingauges is greater than that of the relevant raingauges for the two parameters X1 and X2, highlighting the greater dispersion of the ratios around the optimal value of 1, i.e., less stable calibration parameters for the reference raingauges. Overall, the relevant raingauges led to a better performance and stability of the model parameters.

https://doi.org/10.5194/essd-2023-259
Preprint. Discussion started: 11 October 2023
© Author(s) 2023. CC BY 4.0 License.

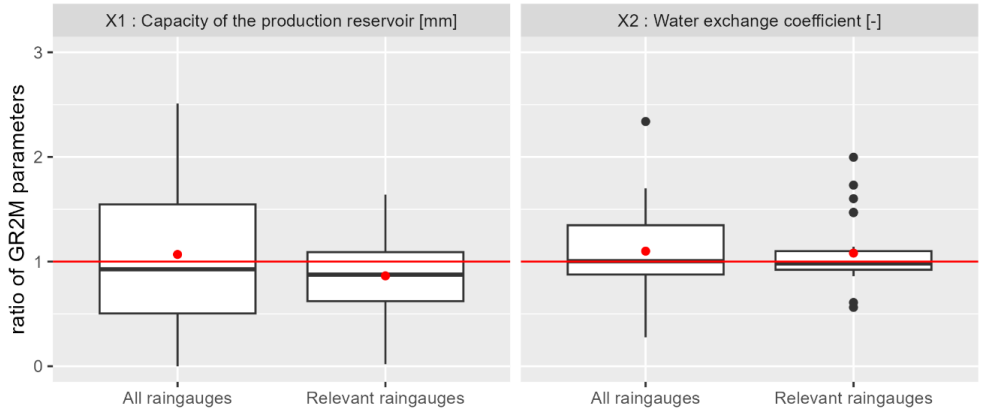

Figure 5 – Ratio of the GR2M calibrated parameters X1 and X2 over the two subperiods for the reference and relevant raingauge combinations.

4.2.3 *Characteristics of relevant raingauge combinations*

Figure *6* shows that the raingauges used for the relevant raingauge combinations are those located at low elevations and with the longest data series. The relatively low percentage of missing data from the relevant raingauges ensured better model stability (see section 4.2.2) and contributed to the improvement in the model performance, especially by reducing the biases between simulated and observed streamflow (improvement in α and β parameters; see section 4.2.1). Raingauges at higher elevations are more difficult to access and are the least maintained, and therefore have very high percentages of missing data. However, the model tends to discard raingauges with high percentages of missing data, which is why the retained/selected raingauges are generally located at lower elevations. There is no clear trend of cumulative rainfall in the selection of relevant raingauges. However, some very wet raingauges (rainfall totals over 180 mm/month) were selected as relevant raingauges.

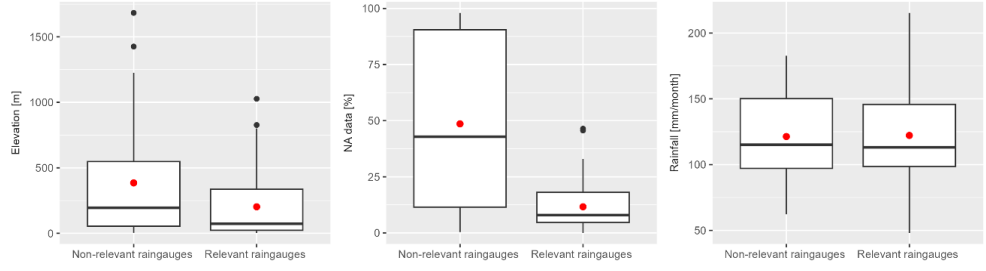

Figure 6 – Distribution of elevations, percentage of missing data, and cumulative monthly rainfall for relevant (40 gauges) and nonrelevant (21 gauges) raingauges.

4.3 Water balance

The average annual water balance, in the form of a Turc–Budyko diagram, was used as another diagnostic tool to verify the hydroclimatic consistency of the data assembled. The results, presented in Figure 7, show that the studied catchments correspond to conservative catchments (points located in the white part of the graph, i.e., Q < P and P - Q < PET), except for the catchments of Rivière du Sud at Camp-Perrin (Q-008) and Rivière Grise (Q-001). More than 90% of the Q-008 catchment is on a calcareous geological formation, and part of the catchment is also affected by karstic aquifers. Therefore, there may be a contribution of water from neighboring catchments that justifies such a high Q/P ratio, but no such study has been conducted to confirm

https://doi.org/10.5194/essd-2023-259
Preprint. Discussion started: 11 October 2023
© Author(s) 2023. CC BY 4.0 License.

or refute this hypothesis. The interpretation of the results for the Q-001 catchment is more difficult, as it may be related to the choice of relevant raingauge combinations for this catchment, or to a real exchange of streamflow with the neighboring catchments, or to a mixture of both. The water balances obtained with the relevant raingauge combinations are shifted to the lower right (blue circles and triangles). This is related to the fact that some of the raingauges used are very wet (see section 4.2.3) and therefore increase the rainfall at the catchment scale. No clear trend was observed between the water balances obtained with observed streamflow and those obtained with simulated streamflow.

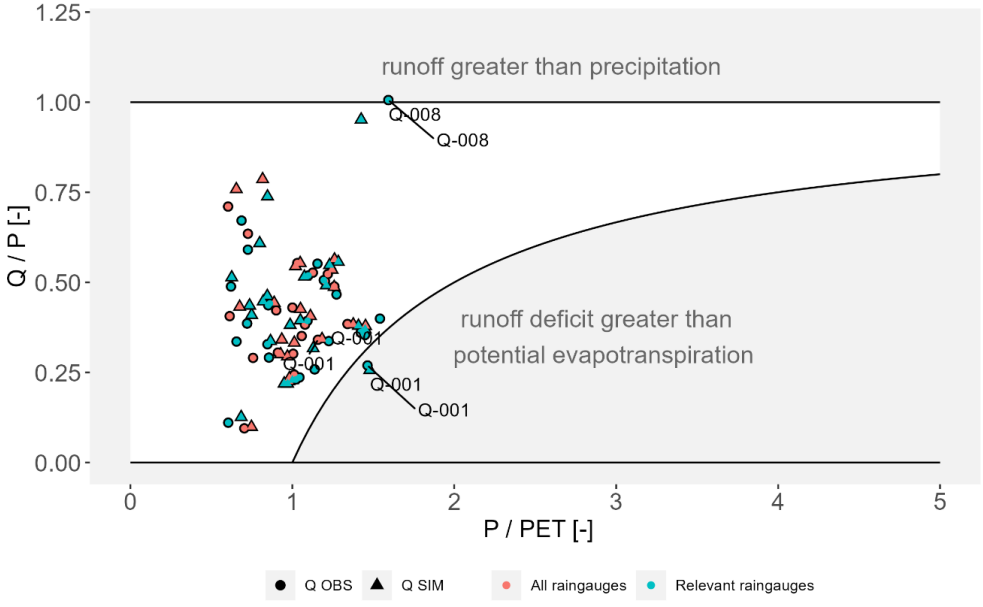

Figure 7 – Average annual water balance in the form of a Turc–Budyko diagram for all 24 catchments. The reference raingauges are shown in red and the relevant raingauges are shown in blue. Observed streamflows are shown as circles and simulated streamflows with parameters calculated over the whole period of available data are shown as triangles.

4.4 Performance of the rainfall–runoff models

Three sets of parameters (see section 3.4) were used to simulate three sets of monthly streamflow for each of the 24 catchments using the GR2M rainfall–runoff model, forced by the relevant raingauge combinations and the PET calculated with digitized air temperatures. The results, presented on the left in Figure 8, show that the KGE scores have a median value of 0.75 in the calibration and 0.67 in the evaluation.

The relevant raingauges have daily data for 21 of the 24 catchments. Therefore, daily streamflow series were simulated by the GR4J model for these 21 catchments. The KGE scores have a median value of 0.57 in the calibration and 0.44 in the evaluation (Figure 8, left). The daily rainfall data used as input to GR4J may partly explain the low KGE values obtained at the daily time step. Indeed, raingauges with high percentages of missing data led to instability and poor performance of the GR2M model in most catchments, which required searching for relevant raingauges to improve the stability and performance of the model at the monthly time step (see section 4.2). However, there is a higher percentage of missing data in the available daily rainfall data than in the monthly data. Furthermore, the limited availability of daily data makes it difficult to improve the performance of the model at the daily time step.

https://doi.org/10.5194/essd-2023-259
Preprint. Discussion started: 11 October 2023
© Author(s) 2023. CC BY 4.0 License.

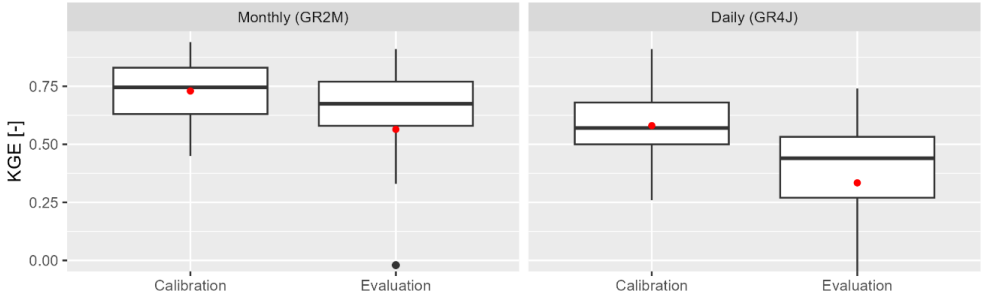

Figure 8 – Synthesis of KGE scores in the calibration and evaluation for modeling with GR2M and GR4J.

4.5 Catchment attributes

The 48 catchment attributes were calculated as described in section 3.5 and Table C2. Results for all attributes are not presented in this paper. Only some climate indices and hydrological signatures are presented.

4.5.1 Hydrological signature at the monthly time step

The observed and simulated mean annual streamflows from GR2M are displayed in Figure *9*. The results show that streamflow is higher in the southwest and north of Haiti and lower in the central part. The simulated streamflow represents well the spatial pattern of the observed streamflow and gives good estimates of the observed mean annual streamflow.

The simulated streamflow represents well the seasonality of the observed streamflow (see Figure *10*). However, the simulated streamflows do not provide good estimates of the monthly streamflow values for the two high streamflow periods in May and November (see Figure *10*). The simulated streamflows overestimate the observed values in May and underestimate them in November. In addition, the simulated streamflows slightly overestimate the low values in January.

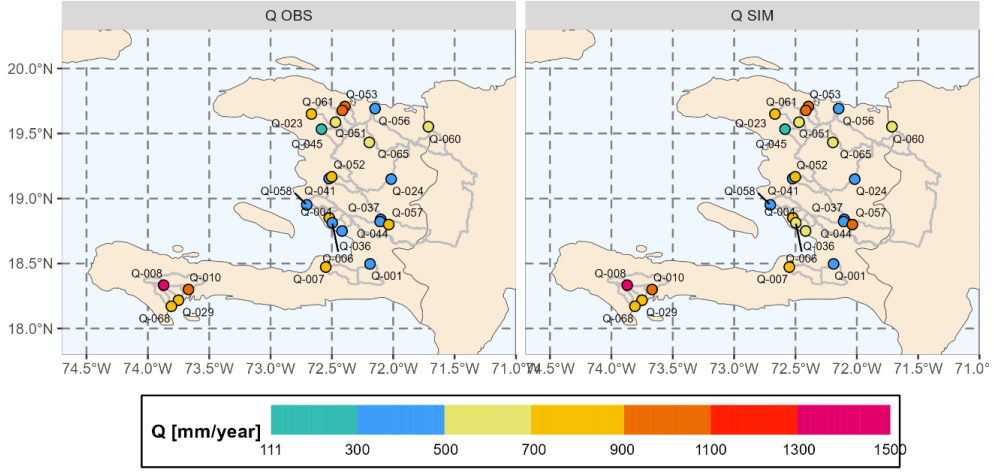

Figure 9 – Spatial distribution of observed mean annual streamflow on the left and simulated streamflow with the GR2M parameters calculated over the entire period of available data on the right.

https://doi.org/10.5194/essd-2023-259
Preprint. Discussion started: 11 October 2023
© Author(s) 2023. CC BY 4.0 License.

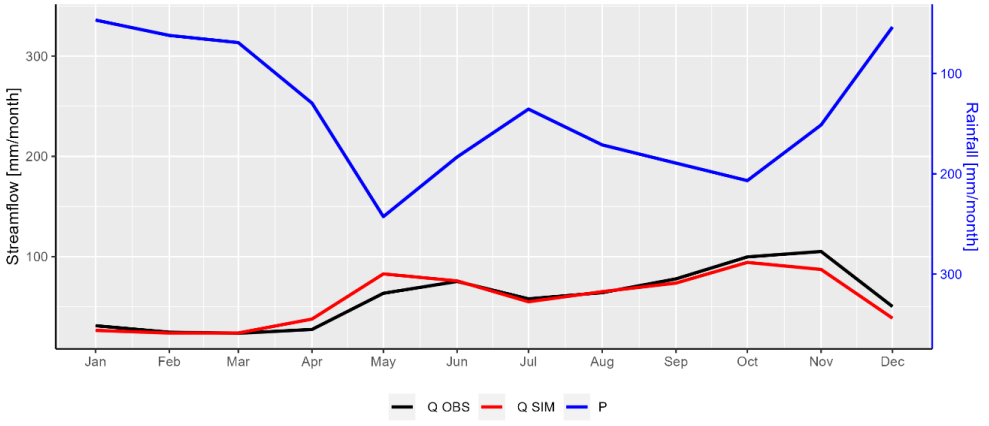

Figure 10 – Seasonality of rainfall (rainfall obtained by combining the relevant raingauges) in blue, observed streamflow in black, and simulated streamflow with the parameters calculated over the entire period of available data in red.

The aridity indices and runoff coefficients are presented in Figure *11*. The aridity indices show the same spatial pattern as the mean annual streamflow (Figure *9*), i.e., they are greater than 1 in the central part of Haiti (arid zone) and lower in the southwest and north (humid zone).

The runoff coefficients are approximately 0.35 for catchments in the central zone and approximately 0.5 in the southwest and north of Haiti. The South River catchment at Camp-Perrin (Q-008), discussed above, has a runoff coefficient greater than 1, meaning that runoff is greater than rainfall. This high runoff coefficient can be explained by the presence of karst aquifers in the Q-008 catchment.

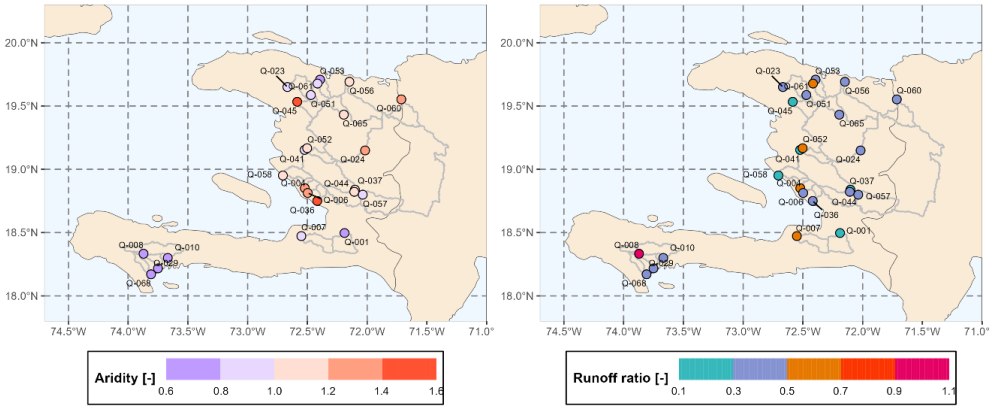

Figure 11 – Aridity index calculated from rainfall series from relevant raingauges on the left, and runoff coefficient calculated from observed streamflow series on the right.

4.5.2 Hydrological signature at daily time step

The hydrological attributes of the simulated and observed streamflow for the 21 selected catchments are summarized in Figure 12. The results show that the simulated streamflows are able to represent average daily streamflow well, underestimate low streamflow (5% quantile), and overestimate high streamflow (95% quantile) and baseflow indices (Pelletier and Andréassian, 2020). These overestimates of high streamflow

https://doi.org/10.5194/essd-2023-259
Preprint. Discussion started: 11 October 2023
© Author(s) 2023. CC BY 4.0 License.

and underestimates of low streamflow result in increased frequencies and durations of simulated high and low streamflow relative to observed streamflow. This poor representation of simulated high and low streamflow is a consequence of the poor performance of the GR4J model for most catchments.

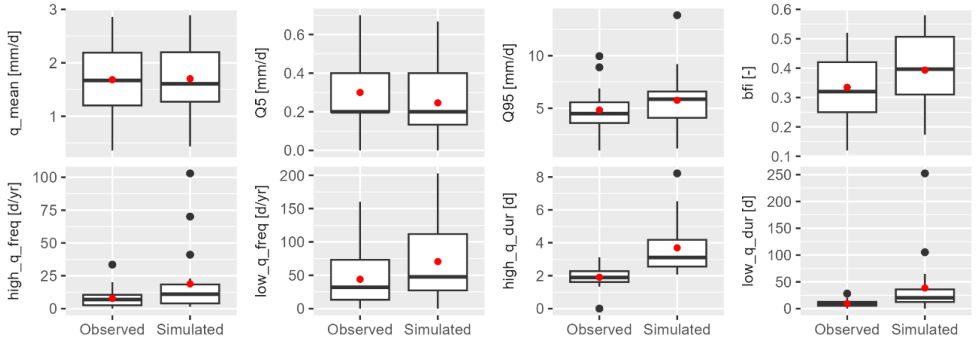

Figure 12 – Summary of hydrological signatures at the daily time step for observed and simulated streamflow and for 21 catchments. From top left: daily mean streamflow, 5% quantiles, 95% quantiles, baseflow, high streamflow frequencies, low streamflow frequencies, high streamflow durations, and low streamflow durations.

4.5.3 Geological and hydrogeological attributes

More than 80% of the total area of the 24 catchments consists of limestone sedimentary rocks (see Figure *13*). These geological formations are the basis for sedimentary aquifers of varying permeability, carbonate aquifers, and karst aquifers (see Figure *14*). These hydrogeological structures favor the exchange of streamflow of greater or lesser magnitude between adjacent catchments, which can result in catchments that are not always hydrologically "closed." In addition to the quality of the data used in our study area, the complex hydrogeology of Haiti may be an explanatory factor for the low KGE values obtained in the validation for several catchments. Unfortunately, few studies have focused on hydrological and hydrogeological modeling in Haiti due to the lack of available data. Simbi could be a starting point for a better understanding of Haitian hydrology.

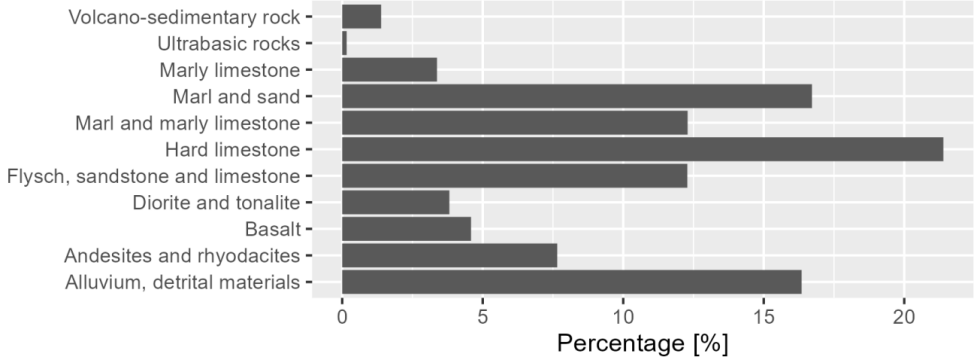

Figure 13 – Percentage of each geological formation in relation to the total area of the 24 catchments.

https://doi.org/10.5194/essd-2023-259
Preprint. Discussion started: 11 October 2023
© Author(s) 2023. CC BY 4.0 License.

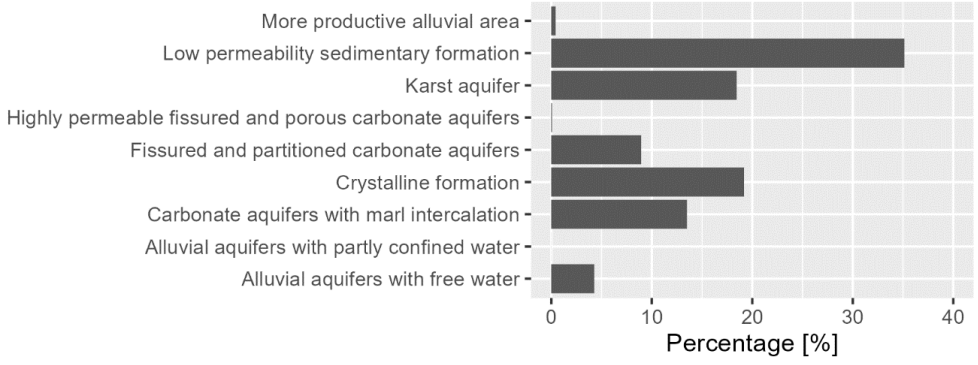

Figure 14 - Percentage of each aquifer type in relation to the total area of the 24 catchments.

4.6 Graphical summary sheets of the Simbi database

The main results are summarized in sheets that highlight the key characteristics of the catchments studied. These summary sheets have been inspired by those prepared by the catchment hydrology research group at INRAE (Brigode et al., 2020). An example is shown in Figure 15 describing the main characteristics of the Cavaillon catchment, which was studied several times after Hurricane Matthew (Mathieu, 2023; Joseph, 2019; Joseph et al., 2018). This catchment has an area of 320 km², half of which is at an elevation above 250 m, with a slope greater than 10°, and overlies a karst aquifer. During the rainy season (April–November), the catchment receives more than 150 mm/month of rainfall and more than 280 mm/month during the peak rainfall in May and November. Streamflows can reach 100 mm/month during May–June and October–November. Simulated streamflows underestimate maximum annual flows with a return period of less than 10 years and overestimate flows beyond 10 years. Simulated streamflows also underestimate low flows (annual minimums). Thus, during flood periods, we can expect daily streamflows of several hundred millimeters, and conversely, during dry periods, streamflows can be on the order of 10 mm/month.

https://doi.org/10.5194/essd-2023-259
Preprint. Discussion started: 11 October 2023
© Author(s) 2023. CC BY 4.0 License.

Open Access Earth System Science Data Discussions

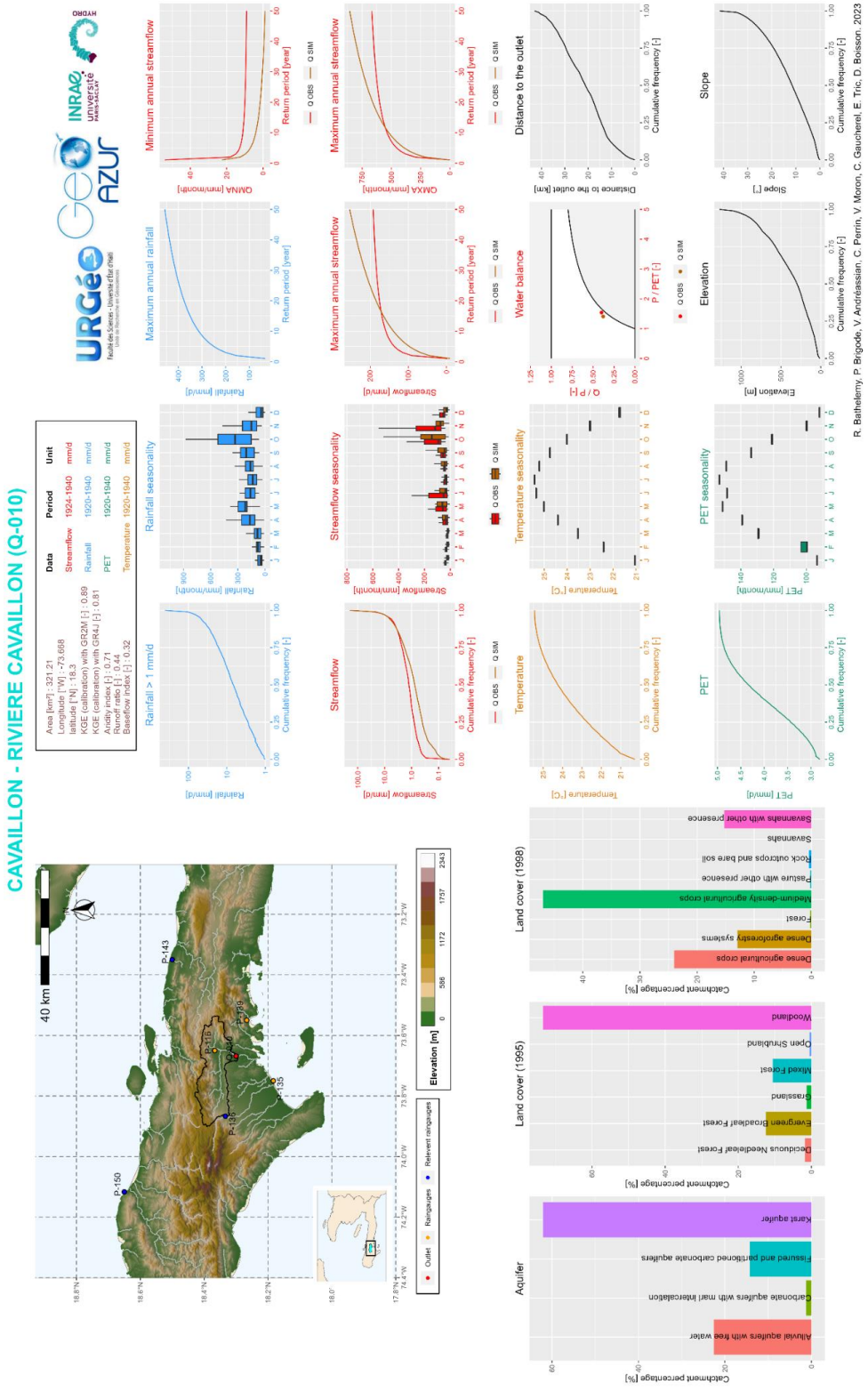

490 Figure 15- Summary sheet of the characteristics of the Cavaillon catchment.

https://doi.org/10.5194/essd-2023-259
Preprint. Discussion started: 11 October 2023
© Author(s) 2023. CC BY 4.0 License.

5 Data availability

The Simbi database is available for download at: https://doi.org/10.23708/02POK6 (Bathelemy et al., 2023). The SIMBI_README.txt file contains a description of the database and the organization of the various files and folders. The 00_OBSERVED_DATA folder contains the observed data (daily streamflow, daily and monthly rainfall, and monthly air temperatures). The 01_CATCHMENT folder contains the contours and the outlets of the 24 catchments. The 02_SIMULATED_STREAMFLOW folder contains the simulated monthly and daily streamflow series. The 03_ATTRIBUTE folder contains all 48 catchment attributes. The 04_MAP folder contains catchment graphical summary sheets summarizing all available data and the main results obtained for each catchment.

6 Conclusion and perspectives

To the best of our knowledge, the hydrological database presented in this article represents the first open access work of an exhaustively documented hydro-meteorological dataset for Haiti. This database, called "Simbi," contains station observations and catchment-scale data. The station observations contain:

1. 59 daily rainfall series available from 1920 to 1940,
2. 156 monthly rainfall series available from 1905 to 2005,
3. 70 daily streamflow series available from 1920 to 1940,
4. 23 monthly air temperature series.

The data at the catchments scale contain:

1. Simulated monthly streamflow series for 24 catchments and simulated daily streamflow series for 21 catchments using three sets of parameters (three simulated streamflow series per catchment) from the GR2M monthly and GR4J daily rainfall–runoff models, and
2. A set of indices that describe a wide range of low, moderate, and extreme rainfall and streamflow characteristics to characterize the hydrological regime and water resources management applications.

The processed database highlights the spatial variability of Haiti's hydrological conditions. The central part of Haiti is associated with relatively low streamflow and high drought coefficients. Conversely, the north and south of Haiti are associated with relatively high streamflow. In fact, large floods are more frequent in these areas (Terrier *et al.*, 2017). The simulated monthly streamflows perform well in representing average streamflow and their spatial variability. However, the model is less effective at the daily time step (KGE score in the evaluation is below 0.5 for most watersheds). This results in poor representation of the frequency or number of consecutive days with high and low streamflow. This may be due to a combination of the quality of the data used and the calcareous geological formations that can create non-conservative catchments that are difficult to model. Moreover, the estimation of relevant raingauge combinations and the simulation are dependent on the model used. A different model may produce different results. Thus, these results should be used with caution.

Our database can be considered a starting point for any hydroclimatic work in Haiti, since it gathers, in addition to the simulated data, all the hydroclimatic data available in Haiti over several decades. It could help to better understand the Haitian climatology in the twentieth century, and to study the evolution of the climate in Haiti for better adaptation to climate change. The database could also contribute to better knowledge of the hydrology of the catchments and help assess the impact of massive deforestation and anarchic urbanization on the hydrological response of the catchments. Frequency analysis methods to estimate flood return periods

https://doi.org/10.5194/essd-2023-259
Preprint. Discussion started: 11 October 2023
© Author(s) 2023. CC BY 4.0 License.

can be considered. Thanks to the availability of streamflow series, this database ushers in perspectives for the application of different approaches to rainfall–runoff modeling. Overall, this hydrological database will contribute to a better understanding of hydrological risk in Haiti. The database will be regularly updated by integrating the historical archives that will later be digitized, making it the most complete hydrological database in Haiti.

Competing interests

The authors declare that they have no conflict of interest.

Author contribution

Conceptualization and methodology: RB, PB, VA, CP. Data curation: RB, VM, CG. Original draft preparation RB. Review and editing: all authors.

Acknowledgments

The authors thank the Bibliothèque Haïtienne des Spiritains (BHS) for providing the paper archive of daily rainfall data and the BVH project for providing the daily streamflow series. Special thanks to the students Eddy-Terson François, Douninio Jeanite, Appollon Jean Philippe, and John Claury Ménélas of the Université d'Etat d'Haïti who contributed to digitizing the daily rainfall data and to the students Kathleen Gerarduzzi, Camille Morillon, and Alexandre Antony of the Université Côte d'Azur who digitized the monthly air temperature data. Olivier Delaigue's work inspired the design of our files, and we extend our thanks to him. Thanks to Isabella Athanassiou for editing the English version of the manuscript.

The authors also thank the CLIMEXHA project (Anticipating Extreme CLIMATE events over HAITI for a sustainable development), which contributed financially to the digitization of the daily rainfall data. This work is part of Ralph Bathelemy's Ph.D. thesis funded by the Anténor Firmin grant from the French Embassy in Haiti, the Institut de Recherche pour le Développement (IRD) through the ARTS grant, and the CARIBACT International Mixed Laboratory.

Appendix A

Verification of the two rainfall databases used was performed by comparing the monthly totals of the digitized daily rainfall series with the monthly rainfall database created by Moron *et al.* (2015). For months where the monthly totals of the two databases differed, a re-verification of the digitized daily rainfall series was carried out, which improved the quality of the digitized daily rainfall data. For some months and stations, the rainfall data produced by Moron et al. were erroneous. The errors in the Moron data are generally of five types:

1. A data entry error during the digitization of this monthly data.
2. Data from some months are confused with data from another station with similar names (e.g., St. Louis du Nord and St. Louis du Sud, Verrettes and Fonds Verrettes), which are often not geographically close.
3. Elimination of some extreme values, thinking that they were input errors. For example, the rainfall was in fact 1196.9 mm at Camp-Perrin (P-136) in October 1933, but the Moron et al. database stated 196.9 mm.
4. Error in calculating monthly totals. In fact, at the end of each month, the monthly rainfall totals were calculated by the raingauge managers, and sometimes there were errors in calculating the monthly totals. However, it is these monthly totals that were used to create the Moron et al. data.
5. Mixing of data from stations located in the same city. Initially, all the raingauges were managed by the observatory of the Petit Séminaire Collège St. Martial, and these raingauges were named after the town in which they were installed. Around 1928, public works began to install stations in the same

https://doi.org/10.5194/essd-2023-259
Preprint. Discussion started: 11 October 2023
© Author(s) 2023. CC BY 4.0 License.

towns as the first stations. This sometimes led to confusion between neighboring stations. For example, the 1920–1930 data for the Hinche station (P-065) are from the observatory station, and the 1931–1940 data are from the public works station. To avoid confusion, only the observatory stations were used in our study because they are more numerous and contain the longest data series.

After this verification process, the corrected Moron et al. database and digitized daily data were used in this study.

Appendix B

GR2M (Mouelhi et al., 2006) is a monthly lumped rainfall–runoff model. Its structure (see Figure B1) combines a production store and a routing store to simulate the hydrological behavior of the catchment. The model has two parameters to optimize during calibration:

1. X1: the production store maximal capacity [mm],
2. X2: the catchment water exchange coefficient [-],

GR4J (Perrin et al., 2003) is a daily lumped rainfall–runoff model. Its structure (see Figure B1) combines a production store and a routing store and unit to simulate the hydrological behavior of the catchment. The model has four parameters to optimize during calibration:

3. X1: the production store maximal capacity [mm],
4. X2: the catchment water exchange coefficient [mm/day],
5. X3: the 1-day maximal capacity of the routing store [mm],
6. X4: the HU1 unit hydrograph time base [days].

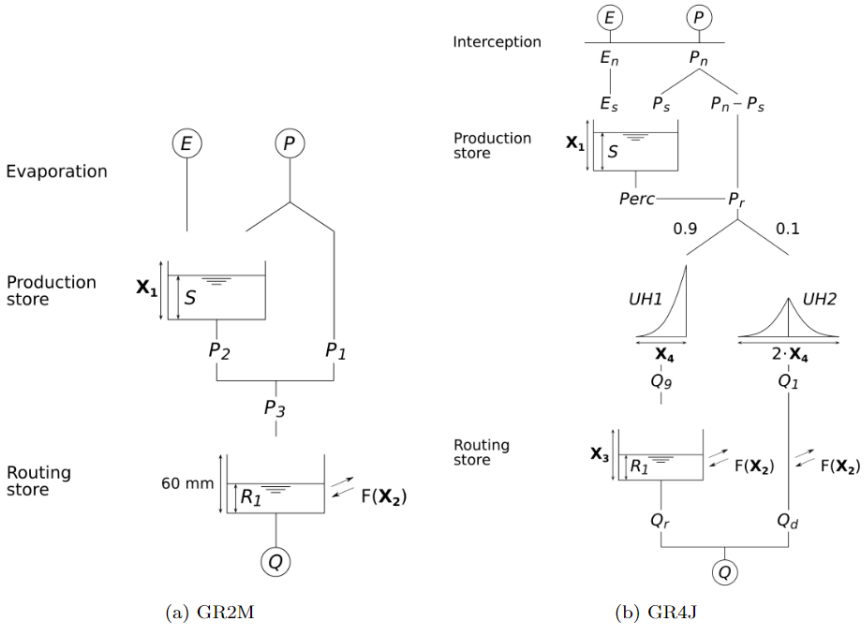

(a) GR2M (b) GR4J

Figure B1 - Diagram of GR2M and GR4J models.

Appendix C

https://doi.org/10.5194/essd-2023-259
Preprint. Discussion started: 11 October 2023
© Author(s) 2023. CC BY 4.0 License.

600 Table C1 – Summary of the number of raingauges used to calculate reference rainfall, the number of combinations of these raingauges, and the most important raingauges for hydrological modeling.

Catchment name	Catchment area [km²]	Catchment code	Number of reference raingauges	Number of combinations without gaps	Relevant raingauges
AMONT DU BASSIN - RIVIERE GRISE	274.33	Q-001	7	110	P-091 P-104 P-095 P-118
ARCAHAIE - RIVIERE MATHEUX	65.65	Q-004	7	92	P-056 P-057 P-059
BASSIN PROBY - RIVIERE COUJOL	78.73	Q-006	6	44	P-054 P-056 P-057 P-059 P-087 P-108
BUISSONNIERE - RIVIERE MOMANCE	239.68	Q-007	7	118	P-091 P-114 P-118
CAMP PERRIN - RIVIERE RAVINE DU SUD	65.73	Q-008	5	8	P-116 P-135 P-136 P-150 P-131
CAVAILLON - RIVIERE CAVAILLON	321.21	Q-010	6	39	P-136 P-143 P-150
GROS MORNE - RIVIERE TROIS-RIVIERES	272.60	Q-023	8	187	P-001 P-004 P-033 P-068 P-070
HINCHE - RIVIERE GUAYAMOUIC	1966.90	Q-024	11	1022	P-075 P-017 P-056 P-059 P-068 P-069 P-070 P-054 P-033
LES CAYES - RIVIERE ISLET	100.77	Q-029	5	19	P-136 P-143 P-150
MESSAYE - RIVIERE TORCELLE	73.00	Q-036	7	88	P-054 P-087 P-093 P-100
MIREBALAIS - RIVIERE ARTIBONITE	7464.22	Q-037	11	1634	P-057 P-060 P-065 P-100 P-068 P-070 P-010 P-069 P-075
P0NT-SONDE - RIVIERE ARTIBONITE	8604.47	Q-041	11	1648	P-056 P-060 P-065 P-066 P-100 P-057 P-069 P-075
PASSE FINE - RIVIERE LA THEME	304.04	Q-044	5	12	P-056 P-057 P-093 P-100 P-108
PASSE JOLY - RIVIERE D'ENNERY	192.13	Q-045	7	107	P-004 P-068 P-028 P-044 P-045 P-033
PLAISANCE - RIVIERE TROIS-RIVIERES	44.84	Q-051	6	43	P-004 P-068 P-070
PONT BENOIT - RIVIERE	137.90	Q-052	8	185	P-057 P-059 P-068 P-056 P-066 P-075 P-053

https://doi.org/10.5194/essd-2023-259
Preprint. Discussion started: 11 October 2023
© Author(s) 2023. CC BY 4.0 License.

ESTERE					
PONT CHRISTOPHE - RIVIERE LIMBE	245.46	Q-053	8	187	P-004 P-009 P-010 P-068 P-044
RIVIERE GRANDE RIV. DU NORD	547.75	Q-056	10	508	P-068 P-009 P-017 P-025 P-027 P-065
PONT PETION - RIVIERE FER-A CHEVAL	479.04	Q-057	8	216	P-062 P-072 P-104
PONT TOUSSAINT - RIVIERE MONTROUIS	168.20	Q-058	10	950	P-028 P-056 P-068 P-057 P-087
OUANAMINTHE - RIVIERE MASSAGRE	315.01	Q-060	4	8	P-057 P-068 P-017
ROCHE HALEINE - RIVIERE LIMBE	128.40	Q-061	8	187	P-004 P-033 P-044 P-068 P-070 P-010 P-009
ST-RAPHAEL - RIVIERE BONYAHA	177.95	Q-065	8	126	P-004 P-009 P-045 P-068 P-010 P-033
TORBECK - RIVIERE TORBECK	95.99	Q-068	4	9	P-136 P-143 P-150

Table C2 - List of catchment attributes used in this study.

Attribute class	**Attribute name**	**Description**	**Unit**
Location and topography	code	catchment identifier	-
	name	Catchment name	-
	Lon_Exu	Longitude of the catchment outlet	°W
	Lat_Exu	Latitude of the catchment outlet	°N
	Lon_Cent	Longitude of the catchment centroid	°W
	Lat_Cent	Latitude of the catchment centroid	°N
	Area	Catchment area	Km²

https://doi.org/10.5194/essd-2023-259
Preprint. Discussion started: 11 October 2023
© Author(s) 2023. CC BY 4.0 License.

	Gravelius	Gravelius coefficient (catchment elongation)	-
	Min_Elev	Minimum catchment elevation	m
	Max_elev	Maximum catchment elevation	m
	Sd_Elev	Standard deviation of catchment elevations	m
	Slope	Average slope of the catchment computed according to Horn (1981)	°
	Hypso_curve	cumulative frequency of catchment elevations	m
Geological characteristics	Lithology	Percentage of the catchment covered by each geologic class	%
	Carb_Rocks_Perc	Percentage of the catchment covered by carbonate sedimentary rocks	%
	Sedim_Perc	Percentage of the catchment covered by sedimentary rocks	%
	Magma_Perc	Percentage of the catchment covered by magmatic rocks	%
Aquifer characteristic	Aquifer	Percentage of the aquifer classes by each catchment	%
Land cover	Cover_95	Percentage of the catchment covered by each landcover class (1995)	%
	Cover_98	Percentage of the catchment covered by each landcover class (1998)	%

https://doi.org/10.5194/essd-2023-259
Preprint. Discussion started: 11 October 2023
© Author(s) 2023. CC BY 4.0 License.

Climatic indices	Aridity	Aridity index: ratio between the rainfall and the potential evapotranspiration (PE)	-
	P_mean	Rainfall average	mm/month
	T_mean	Temperature average	°C
	PE_mean	PE average	mm/month
	P_5_month	Rainfall quantile 5%	mm/month
	T_5_month	Temperature quantile 5%	°C
	PE_5_month	PE quantile 5%	mm/month
	P_95_month	Rainfall quantile 95%	mm/month
	T_95_month	Temperature quantile 95%	°C
	PE_95_month	PE quantile 95%	mm/month
	PMNA5	Yearly minimum of monthly rainfall not exceeded once in 5 years	mm/month
	PMXA10	Yearly maximum of monthly rainfall exceeded once in 10 years	mm/month
Hydrological signatures on a monthly time scale calculated with observed and 3 simulated streamflow	Runoff_Ratio	Runoff coefficient: ratio between the streamflow and the rainfall	-
	Q_mean_month	Mean monthly streamflow	mm/month
	Q_5_month	Streamflow quantile 5%	mm/month
	Q_95_month	Streamflow quantile 95%	mm/month
	QMNA5	Yearly minimum of monthly streamflow not exceeded once in 5 years	mm/month

https://doi.org/10.5194/essd-2023-259
Preprint. Discussion started: 11 October 2023
© Author(s) 2023. CC BY 4.0 License.

	QMXA10	Yearly maximum of monthly streamflow exceeded once in 10 years	mm/month
	GR2M_param	the two parameters of GR2M	-
Hydrological signatures on daily time scale calculated with observed and 3 simulated streamflow	Q_mean_day	Mean daily streamflow	mm/d
	bfi	Baseflow index : ratio between the baseflow volume and the total streamflow volume (Pelletier and Andréassian, 2020)	-
	high_q_freq	Frequency of high-flow days (> 9 times the median daily flow)	d/yr
	high_q_dur	Average duration of high-flow events (number of consecutive days > 9 times the median daily flow)	d
	low_q_freq	Frequency of low-flow days (< 0.2 times the mean daily flow)	d/yr
	low_q_dur	Average duration of low-flow events (number of consecutive days < 0.2 times the mean daily flow)	d
	Q_5_day	Streamflow quantile 5% (low flow)	mm/d
	Q_95_day	Streamflow quantile 5% (high flow)	mm/d
	GR4J_param	the four parameters of GR2M	

https://doi.org/10.5194/essd-2023-259
Preprint. Discussion started: 11 October 2023
© Author(s) 2023. CC BY 4.0 License.

605 Table C3 – Types of lithology, aquifers, and land use.

lithology types	Alluvium, detrital materials
	Andesites and rhyodacites
	Basalt
	Diorite and tonalite
	Flysch, sandstone and limestone
	Hard limestone
	Marl and marly limestone
	Marl and sand
	Marly limestone
	Ultrabasic rocks
	Volcano-sedimentary rock
Acquifer types	Alluvial aquifers with free water
	Alluvial aquifers with partly confined water
	Carbonate aquifers with marl intercalation
	Crystalline formation
	Fissured and partitioned carbonate aquifers
	Highly permeable fissured and porous carbonate aquifers
	Karst aquifer
	Low permeability sedimentary formation
	More productive alluvial area
land use types in 1995	Closed Shrubland
	Cropland
	Deciduous Broadleaf Forest
	Deciduous Needleleaf Forest
	Evergreen Broadleaf Forest

https://doi.org/10.5194/essd-2023-259
Preprint. Discussion started: 11 October 2023
© Author(s) 2023. CC BY 4.0 License.

	Evergreen Needleleaf Forest
	Grassland
	Mixed Forest
	Open Shrubland
	Urban
	Water
	Wooded Grassland
	Woodland
land use types in 1998	Beaches and dunes
	Continuous urban
	Dense agricultural crops
	Dense agroforestry systems
	Discontinuous urban
	Dominant pastures
	Forest
	Industrial areas
	Mangroves
	Medium-density agricultural crops
	Pasture with other presence
	Ports and airports
	Quarry
	River beds and recent alluvium
	Rock outcrops and bare soil
	Saline areas
	Savannahs
	Savannahs with other presence

https://doi.org/10.5194/essd-2023-259
Preprint. Discussion started: 11 October 2023
© Author(s) 2023. CC BY 4.0 License.

	Water plan
	Wetlands

References

Abbaspour, K. C., Faramarzi, M., Ghasemi, S. S., and Yang, H.: Assessing the impact of climate change on water resources in Iran, Water Resources Research, 45, https://doi.org/10.1029/2008WR007615, 2009.

Addor, N., Newman, A. J., Mizukami, N., and Clark, M. P.: The CAMELS data set: catchment attributes and meteorology for large-sample studies, Hydrology and Earth System Sciences, 21, 5293–5313, https://doi.org/10.5194/hess-21-5293-2017, 2017.

Alfieri, L., Lorini, V., Hirpa, F. A., Harrigan, S., Zsoter, E., Prudhomme, C., and Salamon, P.: A global streamflow reanalysis for 1980–2018, Journal of Hydrology X, 6, 100049, https://doi.org/10.1016/j.hydroa.2019.100049, 2020.

Alvarez-Garreton, C., Mendoza, P. A., Boisier, J. P., Addor, N., Galleguillos, M., Zambrano-Bigiarini, M., Lara, A., Puelma, C., Cortes, G., Garreaud, R., McPhee, J., and Ayala, A.: The CAMELS-CL dataset: catchment attributes and meteorology for large sample studies – Chile dataset, Hydrology and Earth System Sciences, 22, 5817–5846, https://doi.org/10.5194/hess-22-5817-2018, 2018.

Andréassian, V., Perrin, C., Michel, C., Usart-Sanchez, I., and Lavabre, J.: Impact of imperfect rainfall knowledge on the efficiency and the parameters of watershed models, Journal of Hydrology, 250, 206–223, https://doi.org/10.1016/S0022-1694(01)00437-1, 2001.

Andréassian, V., Perrin, C., and Michel, C.: Impact of imperfect potential evapotranspiration knowledge on the efficiency and parameters of watershed models, Journal of Hydrology, 286, 19–35, https://doi.org/10.1016/j.jhydrol.2003.09.030, 2004.

Bathelemy, R., Brigode, P., Boisson, D., and Tric, E.: Rainfall in the Greater and Lesser Antilles: Performance of five gridded datasets on a daily timescale, Journal of Hydrology: Regional Studies, 43, 101203, https://doi.org/10.1016/j.ejrh.2022.101203, 2022.

Bathelemy, R., Brigode, P., Andréassian, V., Perrin, C., Moron, V., Gaucherel, C., Tric, E., and Boisson, D.: Simbi database: historical hydro-meteorological time series and catchment attributes in Haiti, 1905-2005, https://doi.org/10.23708/02POK6, 2023.

Beck, H. E., Wood, E. F., Pan, M., Fisher, C. K., Miralles, D. G., Dijk, A. I. J. M. van, McVicar, T. R., and Adler, R. F.: MSWEP V2 Global 3-Hourly 0.1° Precipitation: Methodology and Quantitative Assessment, Bulletin of the American Meteorological Society, 100, 473–500, https://doi.org/10.1175/BAMS-D-17-0138.1, 2019.

Benoit, L., Sichoix, L., Nugent, A. D., Lucas, M. P., and Giambelluca, T. W.: Stochastic daily rainfall generation on tropical islands with complex topography, Hydrology and Earth System Sciences, 26, 2113–2129, https://doi.org/10.5194/hess-26-2113-2022, 2022.

Boisson, D. and Pubellier, M.: Carte géologique à 1/250 000 de la République d'Haïti [Geologic map of the Republic of Haiti at 1/250,000] BME, IMAGEO, CNRS, Paris, 1987.

https://doi.org/10.5194/essd-2023-259
Preprint. Discussion started: 11 October 2023
© Author(s) 2023. CC BY 4.0 License.

Bonhomme, V., Frelat, R., and Gaucherel, C.: Application of elliptical Fourier analysis to watershed boundaries: a case study in Haiti, Géomorphologie : relief, processus, environnement, 19, 17–26, https://doi.org/10.4000/geomorphologie.10100, 2013.

Brigode, P., Brissette, F., Nicault, A., Perreault, L., Kuentz, A., Mathevet, T., and Gailhard, J.: Streamflow variability over the 1881–2011 period in northern Québec: comparison of hydrological reconstructions based on tree rings and geopotential height field reanalysis, Climate of the Past, 12, 1785–1804, https://doi.org/10.5194/cp-12-1785-2016, 2016.

Brigode, P., Génot, B., Lobligeois, F., and Delaigue, O.: Summary sheets of watershed-scale hydroclimatic observed data for France, , https://doi.org/10.15454/UV01P1, 2020.

Brocca, L., Filippucci, P., Hahn, S., Ciabatta, L., Massari, C., Camici, S., Schüller, L., Bojkov, B., and Wagner, W.: SM2RAIN–ASCAT (2007–2018): global daily satellite rainfall data from ASCAT soil moisture observations, Earth System Science Data, 11, 1583–1601, https://doi.org/10.5194/essd-11-1583-2019, 2019.

Burgess, C. P., Taylor, M. A., Spencer, N., Jones, J., and Stephenson, T. S.: Estimating damages from climate-related natural disasters for the Caribbean at 1.5 °C and 2 °C global warming above preindustrial levels, Reg Environ Change, 18, 2297–2312, https://doi.org/10.1007/s10113-018-1423-6, 2018.

Burnash, R. J. C.: The NWS River Forecast System-catchment modeling., Computer models of watershed hydrology., 311–366, 1995.

Butterlin, J.: Geologie generale et regionale de la Republique d'Haiti, Éditions de l'IHEAL, Paris, 1960.

Caillouet, L., Vidal, J.-P., Sauquet, E., Devers, A., and Graff, B.: Ensemble reconstruction of spatio-temporal extreme low-flow events in France since 1871, Hydrology and Earth System Sciences, 21, 2923–2951, https://doi.org/10.5194/hess-21-2923-2017, 2017.

Chagas, V. B. P., Chaffe, P. L. B., Addor, N., Fan, F. M., Fleischmann, A. S., Paiva, R. C. D., and Siqueira, V. A.: CAMELS-BR: hydrometeorological time series and landscape attributes for 897 catchments in Brazil, Earth System Science Data, 12, 2075–2096, https://doi.org/10.5194/essd-12-2075-2020, 2020.

Chokkavarapu, N. and Mandla, V. R.: Comparative study of GCMs, RCMs, downscaling and hydrological models: a review toward future climate change impact estimation, SN Appl. Sci., 1, 1698, https://doi.org/10.1007/s42452-019-1764-x, 2019.

Churches, C. E., Wampler, P. J., Sun, W., and Smith, A. J.: Evaluation of forest cover estimates for Haiti using supervised classification of Landsat data, International Journal of Applied Earth Observation and Geoinformation, 30, 203–216, https://doi.org/10.1016/j.jag.2014.01.020, 2014.

Coron, L., Andréassian, V., Perrin, C., and Le Moine, N.: Graphical tools based on Turc-Budyko plots to detect changes in catchment behaviour, Hydrological Sciences Journal, 60, 1394–1407, https://doi.org/10.1080/02626667.2014.964245, 2015.

Coron, L., Thirel, G., Delaigue, O., Perrin, C., and Andréassian, V.: The suite of lumped GR hydrological models in an R package, Environmental Modelling & Software, 94, 166–171, https://doi.org/10.1016/j.envsoft.2017.05.002, 2017.

Coron, L., Delaigue, O., Thirel, G., Dorchies, D., Perrin, C., Michel, C., Andréassian, V., Bourgin, F., Brigode, P., Moine, N. L., Mathevet, T., Mouelhi, S., Oudin, L., Pushpalatha, R., and Valéry, A.: airGR: Suite of GR Hydrological Models for Precipitation-Runoff Modelling, 2023.

https://doi.org/10.5194/essd-2023-259
Preprint. Discussion started: 11 October 2023
© Author(s) 2023. CC BY 4.0 License.

Coxon, G., Addor, N., Bloomfield, J. P., Freer, J., Fry, M., Hannaford, J., Howden, N. J. K., Lane, R., Lewis, M., Robinson, E. L., Wagener, T., and Woods, R.: CAMELS-GB: hydrometeorological time series and landscape attributes for 671 catchments in Great Britain, Earth System Science Data, 12, 2459–2483, https://doi.org/10.5194/essd-12-2459-2020, 2020.

Croley, T. E. and Hartmann, H. C.: Resolving Thiessen polygons, Journal of Hydrology, 76, 363–379, https://doi.org/10.1016/0022-1694(85)90143-X, 1985.

Crooks, S. M. and Kay, A. L.: Simulation of river flow in the Thames over 120 years: Evidence of change in rainfall-runoff response?, Journal of Hydrology: Regional Studies, 4, 172–195, https://doi.org/10.1016/j.ejrh.2015.05.014, 2015.

Dewandel, B., Lachassagne, P., Bakalowicz, M., Weng, P., and Al-Malki, A.: Evaluation of aquifer thickness by analysing recession hydrographs. Application to the Oman ophiolite hard-rock aquifer, Journal of Hydrology, 274, 248–269, https://doi.org/10.1016/S0022-1694(02)00418-3, 2003.

Dewandel, B., Lachassagne, P., and Qatan, A.: Spatial measurements of stream baseflow, a relevant method for aquifer characterization and permeability evaluation. Application to a hard-rock aquifer, the Oman ophiolite, Hydrological Processes, 18, 3391–3400, https://doi.org/10.1002/hyp.1502, 2004.

Di Piazza, A., Conti, F. L., Noto, L. V., Viola, F., and La Loggia, G.: Comparative analysis of different techniques for spatial interpolation of rainfall data to create a serially complete monthly time series of precipitation for Sicily, Italy, International Journal of Applied Earth Observation and Geoinformation, 13, 396–408, https://doi.org/10.1016/j.jag.2011.01.005, 2011.

Fowler, A.: Assessment of the validity of using mean potential evaporation in computations of the long-term soil water balance, Journal of Hydrology, 256, 248–263, 2002.

Fowler, K. J. A., Acharya, S. C., Addor, N., Chou, C., and Peel, M. C.: CAMELS-AUS: hydrometeorological time series and landscape attributes for 222 catchments in Australia, Earth System Science Data, 13, 3847–3867, https://doi.org/10.5194/essd-13-3847-2021, 2021.

Gaucherel, C., Frelat, R., Lustig, A., Rouy, B., Chéry, Y., and Hubert, P.: Time–frequency analysis to profile hydrological regimes: application to Haiti, Hydrological Sciences Journal, 61, 274–288, https://doi.org/10.1080/02626667.2015.1006231, 2016.

Gaucherel, C., Frelat, R., Salomon, L., Rouy, B., Pandey, N., and Cudennec, C.: Regional watershed characterization and classification with river network analyses, Earth Surface Processes and Landforms, 42, 2068–2081, https://doi.org/10.1002/esp.4172, 2017.

Gaucherel, C., Frelat, R., Polidori, L., El Hage, M., Cudennec, C., Mondesir, P., and Moron, V.: Weak relationships between landforms and hydro-climatologic processes: a case study in Haiti, Hydrology Research, 50, 744–760, https://doi.org/10.2166/nh.2018.041, 2018.

Gupta, H. V., Kling, H., Yilmaz, K. K., and Martinez, G. F.: Decomposition of the mean squared error and NSE performance criteria: Implications for improving hydrological modelling, Journal of Hydrology, 377, 80–91, https://doi.org/10.1016/j.jhydrol.2009.08.003, 2009.

Han, D. and Bray, M.: Automated Thiessen polygon generation, Water Resources Research, 42, https://doi.org/10.1029/2005WR004365, 2006.

https://doi.org/10.5194/essd-2023-259
Preprint. Discussion started: 11 October 2023
© Author(s) 2023. CC BY 4.0 License.

Harrigan, S., Zsoter, E., Alfieri, L., Prudhomme, C., Salamon, P., Wetterhall, F., Barnard, C., Cloke, H., and Pappenberger, F.: GloFAS-ERA5 operational global river discharge reanalysis 1979–present, Earth System Science Data, 12, 2043–2060, https://doi.org/10.5194/essd-12-2043-2020, 2020.

Hedges, S. B., Cohen, W. B., Timyan, J., and Yang, Z.: Haiti's biodiversity threatened by nearly complete loss of primary forest, PNAS, 115, 11850–11855, https://doi.org/10.1073/pnas.1809753115, 2018.

Höge, M., Kauzlaric, M., Siber, R., Schönenberger, U., Horton, P., Schwanbeck, J., Floriancic, M. G., Viviroli, D., Wilhelm, S., Sikorska-Senoner, A. E., Addor, N., Brunner, M., Pool, S., Zappa, M., and Fenicia, F.: CAMELS-CH: hydro-meteorological time series and landscape attributes for 331 catchments in hydrologic Switzerland, Earth System Science Data Discussions, 1–46, https://doi.org/10.5194/essd-2023-127, 2023.

Horn, B. K.: Hill shading and the reflectance map, Proceedings of the IEEE, 69, 14–47, 1981.

Jones, P. D. and Lister, D. H.: Riverflow reconstructions for 15 catchments over England and Wales and an assessment of hydrologic drought since 1865, International Journal of Climatology, 18, 999–1013, https://doi.org/10.1002/(SICI)1097-0088(199807)18:9<999::AID-JOC300>3.0.CO;2-8, 1998.

Joseph, A.: Caractérisation et modélisation des écoulements de crue : application aux inondations de la ville de Cavaillon en Haiti, UCL - Université Catholique de Louvain, 2019.

Joseph, A., Gonomy, N., Zech, Y., and Soares-Frazão, S.: Modelling and analysis of the flood risk at Cavaillon City, Haiti, La Houille Blanche, 68–75, https://doi.org/10.1051/lhb/2018020, 2018.

Khouakhi, A., Villarini, G., and Vecchi, G. A.: Contribution of Tropical Cyclones to Rainfall at the Global Scale, Journal of Climate, 30, 359–372, https://doi.org/10.1175/JCLI-D-16-0298.1, 2017.

Klemeš, V.: Operational testing of hydrological simulation models, Hydrological Sciences Journal, 31, 13–24, https://doi.org/10.1080/02626668609491024, 1986.

Klingler, C., Schulz, K., and Herrnegger, M.: LamaH-CE: LArge-SaMple DAta for Hydrology and Environmental Sciences for Central Europe, Earth System Science Data, 13, 4529–4565, https://doi.org/10.5194/essd-13-4529-2021, 2021.

Kribèche, R.: Etude de la sensibilité d'un modèle pluie-débit à l'exactitude de l'évaporation (modèle GR4J), DEA Thesis, Université Paris XII, Créteil, 1994.

Mathieu, G.: Développement d'une méthodologie pour la cartographie du risque d'inondation : application à la rivière de Cavaillon en Haïti, UCL - Université Catholique de Louvain, 2023.

Mompremier, R., Her, Y., Hoogenboom, G., and Song, J.: Effects of deforestation and afforestation on water availability for dry bean production in Haiti, Agriculture, Ecosystems & Environment, 325, 107721, https://doi.org/10.1016/j.agee.2021.107721, 2022.

Moron, V., Frelat, R., Jean-Jeune, P. K., and Gaucherel, C.: Interannual and intra-annual variability of rainfall in Haiti (1905–2005), Clim Dyn, 45, 915–932, https://doi.org/10.1007/s00382-014-2326-y, 2015.

Mouelhi, S., Michel, C., Perrin, C., and Andréassian, V.: Stepwise development of a two-parameter monthly water balance model, Journal of Hydrology, 318, 200–214, https://doi.org/10.1016/j.jhydrol.2005.06.014, 2006.

https://doi.org/10.5194/essd-2023-259
Preprint. Discussion started: 11 October 2023
© Author(s) 2023. CC BY 4.0 License.

Muller, R. A., Rohde, R., Jacobsen, R., Muller, E., Perlmutter, S., Rosenfeld, A., Wurtele, J., Groom, D., and Wickham, C.: A New Estimate of the Average Earth Surface Land Temperature Spanning 1753 to 2011, Geoinformatics & Geostatistics: An Overview, 2013, https://doi.org/10.4172/2327-4581.1000101, 2014.

Oriani, F., Stisen, S., Demirel, M. C., and Mariethoz, G.: Missing Data Imputation for Multisite Rainfall Networks: A Comparison between Geostatistical Interpolation and Pattern-Based Estimation on Different Terrain Types, Journal of Hydrometeorology, 21, 2325–2341, https://doi.org/10.1175/JHM-D-19-0220.1, 2020.

Oudin, L., Hervieu, F., Michel, C., Perrin, C., Andréassian, V., Anctil, F., and Loumagne, C.: Which potential evapotranspiration input for a lumped rainfall–runoff model?: Part 2—Towards a simple and efficient potential evapotranspiration model for rainfall–runoff modelling, Journal of Hydrology, 303, 290–306, https://doi.org/10.1016/j.jhydrol.2004.08.026, 2005.

Pelletier, A. and Andréassian, V.: Hydrograph separation: an impartial parametrisation for an imperfect method, Hydrology and Earth System Sciences, 24, 1171–1187, https://doi.org/10.5194/hess-24-1171-2020, 2020.

Perrin, C., Michel, C., and Andréassian, V.: Improvement of a parsimonious model for streamflow simulation, Journal of Hydrology, 279, 275–289, https://doi.org/10.1016/S0022-1694(03)00225-7, 2003.

Peterson, T. C., Taylor, M. A., Demeritte, R., Duncombe, D. L., Burton, S., Thompson, F., Porter, A., Mercedes, M., Villegas, E., Fils, R. S., Tank, A. K., Martis, A., Warner, R., Joyette, A., Mills, W., Alexander, L., and Gleason, B.: Recent changes in climate extremes in the Caribbean region, Journal of Geophysical Research: Atmospheres, 107, ACL 16-1-ACL 16-9, https://doi.org/10.1029/2002JD002251, 2002.

Prakash, S.: Performance assessment of CHIRPS, MSWEP, SM2RAIN-CCI, and TMPA precipitation products across India, Journal of Hydrology, 571, 50–59, https://doi.org/10.1016/j.jhydrol.2019.01.036, 2019.

R Core Team: R: A Language and Environment for Statistical Computing, R Foundation for Statistical Computing, Vienna, Austria, 2022.

Reuter, H. I., Nelson, A., and Jarvis, A.: An evaluation of void-filling interpolation methods for SRTM data, International Journal of Geographical Information Science, 21, 983–1008, https://doi.org/10.1080/13658810601169899, 2007.

Salomon, W., Useni Sikuzani, Y., Sambieni, K. R., Kouakou, A. T. M., Barima, Y. S. S., Théodat, J. M., and Bogaert, J.: Land Cover Dynamics along the Urban–Rural Gradient of the Port-au-Prince Agglomeration (Republic of Haiti) from 1986 to 2021, Land, 11, 355, https://doi.org/10.3390/land11030355, 2022.

Slivinski, L. C., Compo, G. P., Whitaker, J. S., Sardeshmukh, P. D., Giese, B. S., McColl, C., Allan, R., Yin, X., Vose, R., Titchner, H., Kennedy, J., Spencer, L. J., Ashcroft, L., Brönnimann, S., Brunet, M., Camuffo, D., Cornes, R., Cram, T. A., Crouthamel, R., Domínguez-Castro, F., Freeman, J. E., Gergis, J., Hawkins, E., Jones, P. D., Jourdain, S., Kaplan, A., Kubota, H., Blancq, F. L., Lee, T.-C., Lorrey, A., Luterbacher, J., Maugeri, M., Mock, C. J., Moore, G. W. K., Przybylak, R., Pudmenzky, C., Reason, C., Slonosky, V. C., Smith, C. A., Tinz, B., Trewin, B., Valente, M. A., Wang, X. L., Wilkinson, C., Wood, K., and Wyszyński, P.: Towards a more reliable historical reanalysis: Improvements for version 3 of the Twentieth Century Reanalysis system, Quarterly Journal of the Royal Meteorological Society, 145, 2876–2908, https://doi.org/10.1002/qj.3598, 2019.

Smith, K. A., Barker, L. J., Tanguy, M., Parry, S., Harrigan, S., Legg, T. P., Prudhomme, C., and Hannaford, J.: A multi-objective ensemble approach to hydrological modelling in the UK: an application to historic drought reconstruction, Hydrology and Earth System Sciences, 23, 3247–3268, https://doi.org/10.5194/hess-23-3247-2019, 2019.

https://doi.org/10.5194/essd-2023-259
Preprint. Discussion started: 11 October 2023
© Author(s) 2023. CC BY 4.0 License.

795 Tarboton, D. G., Watson, D. W., Wallace, R., Schreuders, K. A. T., and Neff, J.: Terrain Analysis Using Digital Elevation Models, 48, 2005.

Tarter, A., Freeman, K. K., Ward, C., Sander, K., Theus, K., Coello, B., Fawaz, Y., Miles, M., and Ahmed, T. T. G.: Charcoal in Haiti: A National Assessment of Charcoal Production and Consumption Trends, World Bank, Washington, DC, https://doi.org/10.1596/31257, 2018.

800 Terrier, M., Bialkowski, A., Nachbaur, A., Prépetit, C., and Joseph, Y. F.: Revision of the geological context of the Port-au-Prince metropolitan area, Haiti: implications for slope failures and seismic hazard assessment, Nat. Hazards Earth Syst. Sci., 14, 2577–2587, https://doi.org/10.5194/nhess-14-2577-2014, 2014.

Terrier, M., Rançon, J.-P., Bertil, D., Chêne, F., Desprats, J.-F., Lecacheux, S., Le Roy, S., Stollsteiner, P., Bouc, O., and Raynal, M.: Atlas des menaces naturelles en Haïti, 2017.

805 Teutschbein, C. and Seibert, J.: Bias correction of regional climate model simulations for hydrological climate-change impact studies: Review and evaluation of different methods, Journal of Hydrology, 456–457, 12–29, https://doi.org/10.1016/j.jhydrol.2012.05.052, 2012.

Tramblay, Y., Rouché, N., Paturel, J.-E., Mahé, G., Boyer, J.-F., Amoussou, E., Bodian, A., Dacosta, H., Dakhlaoui, H., Dezetter, A., Hughes, D., Hanich, L., Peugeot, C., Tshimanga, R., and Lachassagne, P.: ADHI:
810 the African Database of Hydrometric Indices (1950–2018), Earth System Science Data, 13, 1547–1560, https://doi.org/10.5194/essd-13-1547-2021, 2021.